Density Functional Theory Calculation of the Band Alignment of $(10\bar{1}0)$ $In_xGa_{1-x}N$/Water Interfaces

Andrew C. Meng,[†,‡] Jun Cheng,[¶] and Michiel Sprik[*,†]

Department of Chemistry, University of Cambridge, Cambridge CB2 1EW, United Kingdom, Department of Materials Science and Engineering, Stanford University, CA 94305-4034, United States, and Department of Chemistry, University of Aberdeen, Aberdeen AB24 3UE, United Kingdom

E-mail: ms284@cam.ac.uk
Phone: +44-1223-336314. Fax: +44-1223-336362

Abstract

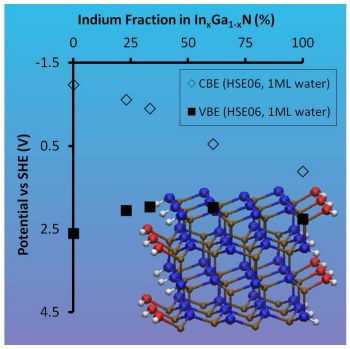

Conduction band edge (CBE) and valence band edge (VBE) positions of $In_xGa_{1-x}N$ photoelectrodes were computed using density functional theory methods. The band edges of fully solvated GaN and InN model systems were aligned with respect to the standard hydrogen electrode using a molecular dynamics hydrogen electrode scheme applied earlier to TiO_2/water interfaces. Similar to TiO_2 we found that the Purdew-Burke-Ernzerhof (PBE) functional gives a VBE potential which is too negative by 1 V. This cathodic bias is largely corrected by application of the Heyd-Scuseria-Ernzerhof (HSE06) hybrid functional containing a fraction of Hartree Fock exchange. The effect of a change of composition was investigated using simplified model systems consisting of vacuum slabs covered on both sides by one monolayer of H_2O. The CBE was found to vary linearly with In content. The VBE, in comparison, is much less sensitive to composition. The data show that the band edges straddle the hydrogen and oxygen evolution potentials for In fractions less than 47 percent. The band gap was found to exceed 2 eV for an In fraction less than 54 percent.

Keywords

Band alignment, InGaN, hydrogen insertion method, water splitting, density functional theory

Introduction

Finding new materials suitable for solar driven water splitting is a major challenge. From theoretical considerations, a semiconductor must have a band gap of 1.23 eV and equilibrium band edge positions that straddle the oxygen evolution and hydrogen evolution potentials in

*To whom correspondence should be addressed
†University of Cambridge
‡Stanford University
¶University of Aberdeen

order to drive water splitting. Taking into account energy losses from kinetic and concentration overpotentials for the overall water splitting reaction, the band gap requirement is actually closer to 2 eV, assuming 0.8 eV is lost per photon absorbed in the material. For the material to be stable under water splitting conditions, its oxidative decomposition potential must be more positive than its valence band edge (VBE), and its reductive decomposition potential must be more negative than its conduction band edge (CBE).[1] The material must be Earth-abundant to be viable for scale-up. Furthermore, it must have significant absorption in the visible spectrum.

This combination of requirements is very stringent, and very few materials satisfy the entire set. Photoelectrodes incorporating GaN have attracted interest recently as satisfying the appropriate band gap and band positions as well as showing promising stability.[2–10] Further motivation for the renewed interest in the (photo)electrochemistry of GaN-electrolyte interfaces[11–13] is the application in pH sensors.[14–16] GaN photoelectrodes have also been the subject of a series of computational studies by Muckerman, Fernandez-Serra and coworkers.[17–23] In a recent paper these authors have turned to the challenging problem of computational band alignment of this material[22] which is also the topic of the present contribution.

Electronic structure calculation methods have already made important contributions to the field of band gap engineering aiming at optimization of light absorption.[24–26] These calculations are usually carried out for homogeneous systems without an interface to an aqueous electrolyte. The established methods of computational surface science have also proven to be very useful. The approach here is to study the electronic structure of a mono or bilayer of adsorbate, in particular of course H_2O, on a photo anode surface, leaving out the bulk electrolyte. The favourite system for this type of studies is TiO_2.[27,28] Such a calculation often gives already a reliable picture of the positions of adsorbates energy levels relative to the VBE and CBE of a semiconductor. Proper band alignment of a photoelectrode, however, must go further. The primary challenge lies in placing the band structure of the electrode with respect to the Standard Hydrogen Electrode (SHE) under conditions as close as possible to the operating conditions of the electrode.

First principles calculation of band alignment of semiconductor heterostructures was pioneered in the late 1980s.[29–32] This calculation proceeds in two steps. First the electrostatic (Hartree) potential profile across the interface in the heterogeneous system is computed using standard DFT methods. The potential in the bulk regions on either side of the interface is "nano" smoothed in order to determine the Hartree potential offset.[32] Next the differences in energy between the VBE or CBE and the average Hartree potential in a homogeneous model system of the two materials is computed and added to the Hartree potential offset. For a semiconductor electrolyte interface additional averaging over the thermal fluctuations of the liquid is required. This calculation is now feasible for fairly large model systems of semiconductor/water interfaces and has been carried out for functionalized Si(111) surfaces[33] and, as already mentioned, the GaN $(10\bar{1}0)$surface.[22] For applications to interfacial electrochemistry an additional step is necessary, namely the determination of the energy of the VBE of liquid water relative to vacuum.[34] As it turns out, this third step is the more challenging part of electrochemical band alignment, which has led to the development of partly empirical schemes trying to avoid this step.[35,36] In the present study of the GaN/water interface we apply an alternative computational hydrogen electrode scheme developed in previous work.[37,38]

Recently, the Perdew-Burke-Ernzerhof (PBE) functional and the Heyd-Scuseria-Ernzerhof (HSE06) hybrid functional were used to calculate the band alignment of $In_xGa_{1-x}N$ surfaces in vacuum for varying In content without explicitly taking into consideration the semiconductor-electrolyte interface.[39–41] We are interested in taking into account the potential shift at the $In_xGa_{1-x}N/H_2O$ interface, as well as looking at the band edge positions in $In_xGa_{1-x}N$ alloys of varying In concentrations as a proof of principle for application

of DFTMD methods to new materials discovery for water splitting applications. For this study, the non polar GaN $(10\bar{1}0)$ surface is chosen since it has been shown to exhibit desirable photocatalytic properties.[17–20,22] We will also compare our DFT calculation to the results of an advanced many body electronic structure method (GW) carried out by Hybertsen and coworkers.[22]

Methods

MD hydrogen electrode: General

The computational standard hydrogen electrode used here to align the electronic energy levels of a solid in contact with water is based on Trasatti's analysis of the hydrogen electrode.[42] Ionization potentials (IP's) and electron affinities (EA's) are in effect referred to the solvation free energy (workfunction) of the proton. This applies to an adiabatic ionization potential (AIP) measured as a redox potential using electrochemical methods as well as vertical ionization potentials determined by photoelectron spectroscopy (PES). To relate the electrochemistry to the spectroscopy Trasatti defined an absolute standard hydrogen potential $U^{\circ}_{\mathrm{H^+/H_2}}(abs)$ accessible to experimental determination. The estimate given in Ref. 42 is $U^{\circ}_{\mathrm{H^+/H_2}}(abs) = 4.44\mathrm{V}$ which is the number we will use in this paper.

The computational standard hydrogen electrode combines density functional based molecular dynamics (DFTMD) with free energy perturbations methods. Following Ref. 43 we will refer to this scheme as the molecular dynamics hydrogen electrode (MDHE). The MDHE method was originally developed for the computation of redox potentials and acidity constants (pKa) of aqueous species in homogeneous solution.[43–47] The MDHE scheme was subsequently applied to the computation of vertical IP's of aqueous species and compared to the corresponding PES data.[46–49] The same methodology was used for the computation of the SHE potential of energy levels and surface pKa's of solids interacting with water. The focus of this work was rutile $TiO_2(110)$.[37,38,50,51] Surface acidity calculations were also carried out for minerals such as silica(SiO_2),[52] gibbsite $(Al(OH)_3)$[53] and clays.[54]

The central reference energy in the MDHE method is not some convenient electronic energy level but the solvation free energy of the proton. This is an expensive calculation. The motivation to opt for this computationally costly approach is the study of proton coupled electron transfer (PCET) reactions.[44,45] The net result of successive electronic ionization and deprotonation of a hydride XH is dehydrogenation ($\mathrm{XH} \rightarrow \mathrm{X} + 1/2\mathrm{H_2}$). This process is the elementary step in many of the energy conversion reactions in organic and inorganic systems. Consistency between the computation of the free energy of electronic ionization and deprotonation is crucial in the DFTMD framework.

We mention one important example which has occupied us in previous work. Both ionization and deprotonation involve a change of net charge which under periodic boundary conditions (PBC) is subject to finite system size errors. Another source of error is the inaccuracy in the DFT approximation, which is a serious concern for electron ionization (involving open shell species)[43,46–49] but much less so for deprotonation (a reaction between closed shell species).[45,47] This enabled us to separate finite system size errors from DFT errors confirming that the DFT error dominates in IP calculation. Similarly, because of the transferability of the MDHE scheme between heterogeneous and homogeneous systems, the energy levels of electrodes can be validated by calculation of benchmark homogeneous redox reactions for which accurate experimental estimates are available. This is an important advantage because the DFT errors in IP's of extended systems can be large. The rather frightening example is the VBE of liquid water. The absolute value in the generalized gradient approximation (GGA) is underestimated by as much as 3.5 eV.[34,38]

MDHE: Technical summary

The MDHE method is designed to align both redox potentials and electronic energy levels with respect to the SHE. While the present application is mainly concerned with electronic energy levels the distinction with redox free energies is relevant and is best explained by first considering the oxidation of an aqueous species X^q in homogeneous solution.

$$X^q \rightarrow X^{q+1} + e^- \tag{1}$$

q is the charge of the species. Our favourite example of such a reaction is the oxidation of the hydroxide ion OH^- ($q = -1$) repeatedly studied in previous work.[46–48] The product is the hydroxyl radical $OH^\bullet$ ($q + 1 = 0$). We want to compute the adiabatic ionization potential AIP_q, which can be formally defined as the free energy for reversible removal of an electron. Free energies are not directly accessible in electronic structure calculation which only deals with total energy differences. However free energy differences can be related to total energy differences using coupling integral methods.[55] A fictitious mapping Hamiltonian $\mathcal{H}_\eta$ is constructed

$$\mathcal{H}_\eta = \eta\mathcal{H}_{q+1} + (1-\eta)\,\mathcal{H}_\mathrm{q} \tag{2}$$

consisting of a linear combination of the atomic Hamiltonian $\mathcal{H}_{q+1}$ of the oxidized state (X^{q+1}) and $\mathcal{H}_q$ of the reduced state (X^q). The coupling parameter connecting the reduced and oxidized states takes the values $0 \leq \eta \leq 1$. The thermodynamic integration is carried out under full 3D periodic boundary conditions (pbc). The result is the free energy for the reversible removal of an electron from the periodic model system

$$\mathrm{AIP}_q(\mathrm{pbc}) = \int_0^1 d\eta\, \langle \Delta E_q(\mathrm{pbc}) \rangle_\eta \tag{3}$$

$\Delta E_q = E_{q+1} - E_q$ is the vertical IP of X^q computed from total energy differences. The brackets denote a thermal average over the canonical ensemble generated by $\mathcal{H}_\eta$.

The absolute value of the vertical ionization energy ΔE_q(pbc) in Eq. 3, and by implication AIP_q(pbc), has no physical meaning. The reason is that the reference of electrostatic energy under PBC is undetermined. Only relative values for charge transfer (CT) reactions can be compared to experiment. The electron removed from the oxidized species in CT remains in the system. It is passed to an oxidant. The net change of charge is zero. However, we can eliminate an electron from the system at zero net charge if we also take out a proton (PCET).

$$X^q + H^+(\mathrm{aq}) \rightarrow X^{q+1} + \frac{1}{2}H_2(\mathrm{g}) \tag{4}$$

The free energy change of reaction Eq. 4, divided by the unit charge e_0, is the redox potential U_q°(she) of the X^{q+1}/X^q couple vs SHE. U_q°(she) is obtained from the AIP of Eq. 3 as

$$U_q^\circ(\mathrm{she}) = \frac{1}{e_0}\mathrm{AIP}_q(\mathrm{pbc}) - U^\circ_{\mathrm{H^+/H_2}}(\mathrm{pbc}) \tag{5}$$

$U^\circ_{\mathrm{H^+/H_2}}$(pbc) is the hydrogen electrode potential for the periodic model cell.

$$e_0 U^\circ_{\mathrm{H^+/H_2}}(\mathrm{pbc}) = \mu^{g,\circ}_{\mathrm{H^+}} - \mathrm{W}_{\mathrm{H^+}}(\mathrm{pbc}) + \Delta E_\mathrm{zp} \tag{6}$$

$\mu^{g,\circ}_{\mathrm{H^+}}$ and ΔE_zp are numerical constants which we specify first.[45] $\mu^{g,\circ}_{\mathrm{H^+}}$ is the formation energy of a gas-phase proton defined as the standard free energy change of $1/2\mathrm{H_2} \rightarrow \mathrm{H^+(g)} + e^-$. $\mu^{g,\circ}_{\mathrm{H^+}} = 15.81$ eV if we use $c^\circ = 1\,\mathrm{M}$ rather than $p^\circ = 1\,\mathrm{bar}$ as the gas-phase standard state. ΔE_zp is a correction for the proton zero point motion. We take $\Delta E_\mathrm{zp} = 0.35$ eV.

$\mathrm{W}_{\mathrm{H^+}}$(pbc) in Eq. 6 is the central quantity computed in the MDHE method. $\mathrm{W}_{\mathrm{H^+}}$(pbc) is the PBC work function of the proton, ie. the reversible work for removing a proton from the PBC model system. This system must have *the same* composition and dimensions as the system for which AIP_q of Eq. 3 is computed.[38,43] $\mathrm{W}_{\mathrm{H^+}}$(pbc) is evaluated using a thermodynamic integral similar to Eq. 3

$$W_{\mathrm{H^+}}(\mathrm{pbc}) = \int_0^1 d\eta\, \langle \Delta E_{\mathrm{H_3O^+}}(\mathrm{pbc}) \rangle_\eta \tag{7}$$

$\Delta E_{\mathrm{H_3O^+}}$ is the energy for vertical deprotonation of a hydronium ion (H_3O^+). The modeling of desolvation of H^+ by deprotonation of H_3O^+

is an approximation originally introduced for the calculation of acidity constants.[56] The implementation and justification of this scheme is outlined in detail in Refs. 44 and 45. We reiterate that $W_{\mathrm{H^+}}(\mathrm{pbc})$ is specific to the periodic model system. Just as for AIP_q of Eq. 3, its absolute value has no physical meaning. Only the sum $\mathrm{AIP}_q(\mathrm{pbc}) + \mathrm{W}_{\mathrm{H^+}}(\mathrm{pbc})$ entering Eq. 5 is physical.

Unlike averages of the ionization energy $\langle \Delta E_q \rangle_\eta$ at intermediate values of the coupling parameter η in the thermodynamic integral of Eq. 3 averages $\langle \Delta E_q \rangle_\eta$ at the end points $\eta = 0$ and $\eta = 1$ are observable spectroscopic energies. In the energy gap at $\eta = 0$ we recognize the vertical ionization potential IP_q of X^q. Again the absolute value relative to vacuum is not known in a system with full 3D periodicity. However, subtracting the PBC hydrogen potential of Eq. 6 gives IP_q relative to SHE.

$$\mathrm{IP}_q(\mathrm{she}) = \langle \Delta E_q \rangle_{\eta=0} - e_0 U^\circ_{\mathrm{H^+/H_2}} \qquad (8)$$

where it is now understood that vertical ionization energies and work functions without an explicit indication of the energy reference are evaluated under PBC conditions. The (pbc) argument has accordingly been suppressed in Eq. 8. In the same simplified notation the vertical electron affinity of EA_{q+1} of the oxidized product X^{q+1} referred to the SHE is obtained as

$$\mathrm{EA}_{q+1}(\mathrm{she}) = \langle \Delta E_q \rangle_{\eta=1} - e_0 U^\circ_{\mathrm{H^+/H_2}} \qquad (9)$$

Without structural relaxation $\mathrm{IP}_q(\mathrm{she}) = \mathrm{EA}_{q+1}(\mathrm{she})$. This identity strictly holds whatever the level of the approximation of the DFT calculation, provided the IP and EA are computed from total energy differences as implied by Eq. 3. The quantity $\mathrm{IP}_q(\mathrm{she}) - \mathrm{EA}_{q+1}(\mathrm{she}) = 2\lambda$ contains crucial information: It quantifies the reorganization energy λ of the solvent and has been determined using DFTMD for a number of (small) aqueous solutes.[43,47] Reorganization energies for these species are large (2 eV or more).

After the detour through the redox chemistry of homogeneous solutions we are ready to address the problem of alignment of the band edges of a semiconductor electrode. This is in principle no different. The species X^q in Eq. 1 becomes an extended neutral solid X ($q = 0$) in contact with water. $\langle \Delta E_0 \rangle_{\eta=0}$ in Eq. 8 can then be interpreted as the thermal average of the vertical IP of solid X. Eq. 8 gives now the position of the valence band edge (VBE) relative to the SHE after a change of sign. Hence we can write

$$\mathrm{VBE}(\mathrm{she}) = -\langle \Delta E_0 \rangle_{\eta=0} + e_0 U^\circ_{\mathrm{H^+/H_2}} \qquad (10)$$

where the proton is removed from the solution away from the interface where bulk water conditions can be assumed to prevail.

We saw that aligning the VBE of a solid with respect to the SHE is an application of Eq. 8 for $q = 0$. Similarly we can obtain the position of the CBE vs SHE from Eq. 9 by setting $q = -1$. Changing sign we can therefore write

$$\mathrm{CBE}(\mathrm{she}) = -\langle \Delta E_{-1} \rangle_{\eta=1} + e_0 U^\circ_{\mathrm{H^+/H_2}} \qquad (11)$$

This is similar to the reduction of $\mathrm{OH}^\bullet$ to OH^- discussed in Refs. 46,47. The neutral species plays the role of the oxidized state which is represented by the $\eta = 1$ limit of the mapping hamiltonian of Eq. 2.

Eqs. 10 and 11 may seem unnecessarily formal. In practice $-\langle \Delta E_0 \rangle_{\eta=0}$ in Eq. 10 can be replaced by the energy of the highest occupied molecular orbital (HOMO) which will be denoted by ϵ_{HOMO}. For finite systems (molecules, clusters) this is usually a bad approximation because of the infamous delocalization error in approximate density functionals. For semiconductors (in absence of point defects) the relation holds to a good approximation. Excess holes in these systems are delocalized. This also means that if holes do localize as they do in TiO_2 (see for example Ref. 57) , the electronic structure of the defect can be regarded as a finite system and estimates of the ionization energy from the HOMO and vertical total energy differences will show substantial discrepancies. Similarly $-\langle \Delta E_{-1} \rangle_{\eta=1} \approx \epsilon_{\mathrm{LUMO}}$ in Eq. 11 where the LUMO is the lowest unoccupied molecular orbital. However, the q, η

mapping Hamiltonian formalism makes it easier to see the relation to the adiabatic band edges which are the formal equivalent to redox free energies. The adiabatic ionization potential (is redox potential) for a species in homogeneous solution is given by Eq. 5 with the AIP_q(pbc) given by Eq. 3. Similarly we can define for the solid

$$\mathrm{AIP(she)} = \int_0^1 d\eta \, \langle \Delta E_0 \rangle_\eta - e_0 U^\circ_{\mathrm{H^+/H_2}} \quad (12)$$

The corresponding expression for the adiabatic electron affinity is

$$\mathrm{AEA(she)} = \int_0^1 d\eta \, \langle \Delta E_{-1} \rangle_\eta - e_0 U^\circ_{\mathrm{H^+/H_2}} \quad (13)$$

Without structural relaxation AIP = −VBE. Finite values of AIP + VBE are a signature of hole trapping which has been observed for TiO_2 when treated at the hybrid GGA-Hartree Fock exchange level of approximation.[57] The question we will have to answer in this paper is whether the same happens to holes in GaN. Similarly trapping of excess electrons leads to finite values of AEA + CBE. We reiterate that AIP(she) of Eq. 12 and AEA(she) of Eq. 13 are not the enthalpies of holes and excess electrons but electrochemical redox levels. This distinction is particularly relevant for ionizable surface states which may give rise to Fermi level pinning at semiconductor liquid junctions.[58]

We conclude this section with a further technical point. In the above outline of the MDHE scheme it was emphasized that electron and proton must be removed or inserted in the same model supercell. Only then the arbitrary offset in the reference of the electrostatic potential under PBC cancels.[38,43,47] Simultaneous removal of an electron-proton pair is referred to as the full reaction scheme. Cancellation of the electrostatic potential bias can also be achieved in a half reaction scheme in which electron and proton are removed sequentially. This can save computer time because the same proton workfunction can be reused for different redox reactions in the same cell. Full and half reaction scheme are not strictly equivalent. The number of charged particles in the model systems is different and therefore the corresponding electrostatic interactions. However these interactions are strongly screened in aqueous systems and in practice these effects turn out to be relatively small and can often be ignored.

DFTMD method

All electronic structure calculations were carried out using the CP2K/QUICKSTEP[59,60] package. The DFTMD simulations were based on the Born-Oppenheimer dynamics method as implemented in CP2K. One-electron orbitals (Γ point only) are represented in a Gaussian-type double-ζ basis with one set of polarization functions (DZVP) re-expanded as plane waves with a 280 Ry cutoff. Core electrons are accounted for by analytic Goedecker-Teter-Hutter (GTH) pseudopotentials,[61,62] including all 10 d electrons for Ga and In. The DFT was implemented at both the generalized gradient approximation level with the PBE functional,[63] and the hybrid functional level (HSE06[64]). Exact exchange under periodic boundary conditions was implemented using the auxiliary density matrix method of Ref. 65. Convergence criteria for electronic gradient and total energy were set to 3×10^{-7} a.u. and 10^{-13} a.u. respectively. The time step for the Born-Oppenheimer DFTMD propagation was 0.5 fs.

Model systems

Fully solvated systems. Free energy calculations for fully solvated systems were performed in a periodic slab geometry of alternating solid and water layers. Only the pure binary compounds GaN and InN were investigated in full solvation mode. The solid slabs were 8 atomic layer thick in $(10\bar{1}0)$ orientation. Lattice constants of $a = 3.190$Å and $c = 5.189$Å for GaN and $a = 3.536$Å and $c = 5.709$Å for InN were used.[66,67] Slab supercells for both GaN and InN consisted of 48 formula units and measured $3a \times 2c$ in the xy directions and 8 atomic layers plus a gap to accommodate water molecules in the z direction. The GaN MD supercell dimensions were 9.5700Å × 10.3780Å × 27.1707Å, and the InN MD supercell dimen-

sions were 10.6080AA $\times$ 11.4180AA $\times$ 28.400Å. The gap in the z direction was filled with 44 water molecules for both GaN and InN; this included one monolayer (6 molecules) adsorbed on each $(10\bar{1}0)$ surface and 32 molecules at approximately the bulk density, thus simulating full water solvation. To equilibrate the adsorbed water monolayers, several hundred geometry optimization iterations were executed, followed by MD for $\approx$ 100 fs. IP and EA calculations using the PBE functional were equilibrated for 2 ps at a temperature of 330 K using a Nose thermostat, and a cumulative average was recorded over $\approx$ 5 ps. The HSE06 hybrid functional was applied to data pre-converged using the PBE functional and a cumulative average was recorded over time periods ranging from $200 - 500$ fs. Thermodynamic integrals were calculated using a trapezoidal approximation sampling the total energy at $\eta = 0.0, 0.5,$ and 1.0. Ionization potentials were calculated using the half-reaction scheme (see MDHE section) which is more convenient for oxidation reactions. Electron affinities were calculated using the full reaction scheme.

Bulk solids. For reference purpose we also carried out calculations on bulk GaN and InN. For GaN, several different supercell sizes were used: $3a \times 2c$ in the xy directions and 8 atomic layers in the z direction (9.5700Å $\times$ 10.3780Å $\times$ 11.0505Å); $4a \times 4c$ in the xy directions and 16 atomic layers in the z direction (12.7600Å $\times$ 20.7560Å $\times$ 22.1010Å); and $6a \times 6c$ in the xy directions and 24 atomic layers in the z direction (19.1400Å $\times$ 31.1340Å $\times$ 33.1515Å). The density of states and the band gap were calculated for the PBE functional for all supercell sizes. For the HSE06 functional only the smallest supercell size was considered due to high cost of computing exact exchange. For InN, the supercell dimensions measured $3a \times 2c$ in the xy directions and 8 atomic layers in the z direction (10.6080Å $\times$ 11.4180Å $\times$ 12.2491Å). The band gap was calculated for the PBE functional and HSE06 hybrid functional.

Mono layer covered slabs in vacuum. Model systems of mixed $In_xGa_{1-x}N$ composition consisted of $(10\bar{1}0)$ oriented slabs with one adsorbed water monolayer on both surfaces. Slab supercells for all $In_xGa_{1-x}N$ slabs consisted of 48 formula units and measured $3a \times 2c$ in the xy directions and 8 atomic layers plus a gap to accommodate surface adsorbed waters and $a \approx 10$Å vacuum region in the z direction. Preparation of equilibrated, adsorbed water monolayers on $In_xGa_{1-x}N$ slabs was similar to the preparation of water monolayers for fully solvated GaN and InN slabs. Alloys with $x = 0.00\%, 22.92\%, 33.33\%, 60.87\%,$ and 100.00% were prepared with In substitution at Ga sites determined by a random number generator in Mathematica. The In distribution in the atomic layers was approximately uniform: the standard deviation of the number of In atoms in each atomic layer was approximately 1 for all prepared $In_xGa_{1-x}N$ coordinates. A linear interpolation between GaN and InN was used to obtain an initial guess for unit cell vector optimization. For $x = 22.92\%$, the supercell dimensions measured 9.9010Å $\times$ 10.7300Å $\times$ 21.4060Å; for $x = 33.33\%$, the supercell dimensions measured 9.9160Å $\times$ 10.729Å $\times$ 21.4430Å; and for $x = 60.87\%$, the supercell dimensions measured 10.4530Å $\times$ 11.3450Å $\times$ 21.927Å. Electronic structure calculations were executed using both the PBE functional and HSE06 hybrid functional.

The dependence of electronic structure on slab thickness was studied for both GaN and InN slabs covered with 1ML of water. Slab supercells measured $3a \times 2c$ in the xy directions. Using the z dimensions for 8 atomic layers as the starting point, supercells with 9, 10, 11, 12, 13, 16, 20, and 24 atomic layers were generated for GaN and supercells with 9, 10, 11, 12, 14, 16, 20, and 24 atomic layers were generated for InN. For supercells with 16 or fewer atomic layers, both the PBE functional and HSE06 hybrid functional were used, and for supercells with more than 16 layers, only the PBE functional was used.

To align the energy levels of monolayer covered slabs we apply the standard scheme of computational surface science . The surfaces are apolar and covered on both sides by a monolayer. The geometry is symmetric with vanishing net dipole moment. It can therefore be assumed that the periodic images of the wet

slabs can be decoupled by separating them by a sufficiently large vacuum region. The vertical VBE and CBE are obtained from the energy of the HOMO and LUMO using the asymptotic plateau of the Hartree potential in the vacuum slab as reference. The consensus in surface science is that these energies represent the alignment with respect to vacuum which are converted to potentials vs SHE by simply adding the 4.44 eV, the experimental absolute SHE potential.[42]

Results

Fully solvated systems

Before presenting the results on the alignment of VBE and CBE we first analyze the density of states (DOS) of the fully solvated system represented in the usual way, namely aligned with respect to the HOMO. The DOS is shown in Fig. 1 together with projections on various constituent atomic states. No gap states are observed. As expected, we see that N p orbitals are the main component of the valence band and that the Ga s and p orbitals together constitute the dominant contribution to the conduction band. The valence band has some Ga d character, although the main Ga d density of states is below the VBE. Similarly, the conduction band has some admixture of N p orbitals. We further observe some O p character near the VBE, which could be interpreted as the signature of coupling to adsorbed water. However because of the overlap between the O p band of the bulk solvent and N p band of the solid, it is difficult to distinguish between adsorbed water and bulk solvent without a more detailed analysis. The O p contribution to the conduction band is small compared to the Ga s and p contributions.

Proceeding next with the absolute alignment of the HSE06 levels we first give the raw PBC adiabatic IP (Eq. 3) and corresponding proton work function $W_{\mathrm{H^+}}$ (Eq. 7) computed for the same unit cell and composition in the half reaction scheme. We found that for GaN, $\mathrm{AIP}_{\mathrm{GaN}}(\mathrm{pbc}) = 0.27$ eV and $W_{\mathrm{H^+}}(\mathrm{pbc}) = 18.10$ eV. Substituting the computed $W_{\mathrm{H^+}}(\mathrm{pbc})$ in Eq. 6 gives $U^{\circ}_{\mathrm{H^+/H_2}}(\mathrm{pbc}) = -1.94$ V. Finally inserting in Eq. 12 we obtain AIP(she) = 2.21 eV corresponding to an adiabatic VBE at 2.21 V vs SHE (This calculation is explained in more detail in the supporting information). The InN ionization energies are is close to those of GaN: $\mathrm{AIP}_{\mathrm{InN}}(\mathrm{pbc}) = -0.38$ eV with $W_{\mathrm{H^+}}(\mathrm{pbc}) = 18.34$ eV. Applying the same conversion to the VBE of InN at yields 1.80 eV vs. SHE. The HSE06 results are compared to the corresponding PBE estimates in Table 1.

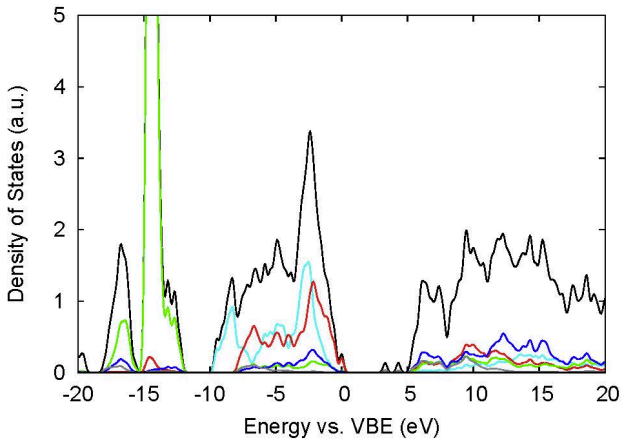

Figure 1: Density of states for a fully water solvated GaN slab using the HSE06 hybrid functional. Zero energy is aligned to the VBE. The color legend is as follows: Blue Ga4p, grey Ga4s, green Ga3d, red N2p, turquoise O2p. The total density of states is indicated by the black curve.

As mentioned the full reaction scheme was used for the CBE calculation. This procedure directly delivers the sum of the adiabatic electron affinity $\mathrm{AEA}_{\mathrm{GaN}}(\mathrm{pbc})$ of Eq. 13 and the PBC proton workfunction (see also supporting information). We find $\mathrm{AEA}_{\mathrm{GaN}}(\mathrm{pbc}) + W_{\mathrm{H^+}}(\mathrm{pbc}) = 14.79$ eV for GaN. InN has a higher EA: $\mathrm{AEA}_{\mathrm{InN}}(\mathrm{pbc}) + W_{\mathrm{H^+}}(\mathrm{pbc}) = 16.60$ eV. The resulting adiabatic GaN CBE is -1.37 eV vs. SHE compared to the more positive InN CBE at 0.44 eV vs SHE. Consistent with experiment InN has a narrower band gap than GaN. The EA free energy calculations are again listed in Table 1 together with experimental estimates. The adiabatic band edges are also shown in the level scheme of Fig. 2.

Table 1: Alignment of the valence band edge (VBE) and conduction band edge (CBE) of GaN, InN and some of their alloys in contact with water. Energies are represented as electrode potentials in Volt with respect to the standard hydrogen electrode (SHE). VBE and CBE have been computed for a slab of solid material with two levels of hydration: in vacuum covered on both side with a monolayer of water (ML) and fully solvated. For the presentation in the form of a level scheme see Fig. 2. The GW results labeled (a) are taken from Ref. 22 (see text). The data labeled (b),[11] (c),[12] (d)[13] and (e)[68,69] are experimental estimates at the pH of 7 (see discussion).

		VBE				CBE			
In %	surface	PBE	HSE	GW$^{(a)}$	exp.	PBE	HSE	GW$^{(a)}$	exp.
0%	ML	1.69	2.60	2.98		−0.66	−0.97	−1.02	
(GaN)	solvated	1.43	2.21	3.19	2.14$^{(b)}$, 2.55$^{(c)}$	−0.94	−1.37	−0.81	−0.86$^{(b)}$, −1.26$^{(c)}$
					2.37$^{(d)}$				−1.00$^{(d)}$
22.92%	ML	1.55	2.05			0.01	−0.61		
33.33%	ML	1.40	1.96			0.14	−0.40		
60.87%	ML	1.40	1.97			0.82	0.45		
100%	ML	1.34	2.25			0.98	1.11		
(InN)	solvated	1.05	1.80		1.22$^{(e)}$	0.65	0.44		0.53$^{(e)}$

Table 1 also quotes the GW estimates as obtained in Ref. 22 for GaN. The band edges in this calculation are computed relative to the VBE of liquid water using the Hartree potential line up method (see introduction) which is then aligned with respect to vacuum by a GW calculation of the IP of water (see also Ref. 34). For the purpose of comparison to our results and experiment, the GW IP's have been converted to a VBE vs SHE by subtracting the experimental absolute hydrogen potential (4.44 V).[42] The CBE listed for GW was obtained by adding the GW bulk band gap of 4.00 eV as given in Ref. 22. Comparison to the DFT results is deferred to the last section of the paper, the conclusion.

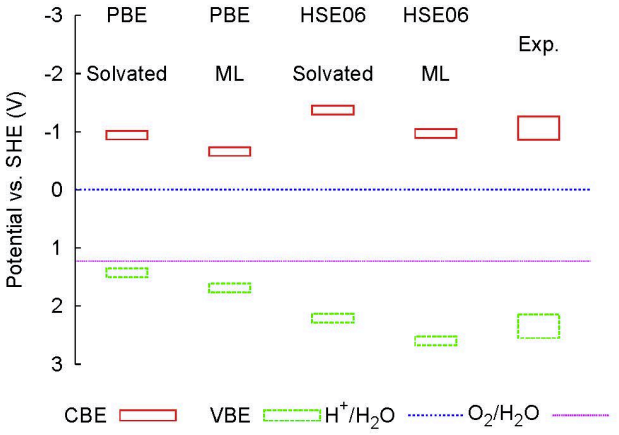

Figure 2: Effect of interface type and density functional on GaN band alignment. Data taken from Table 1.

1 ML H_2O on $(10\bar{1}0)$ $In_xGa_{1-x}N$

A $(10\bar{1}0)$ GaN surface unit consists of a pair of atoms, one Ga and one N, each with one vacant coordination site. For a clean surface, mid-gap electronic states are observed to reduce the energy gap between HOMO and LUMO from 2.98 eV in a bulk structure to 1.56 eV for 8 atomic layers (HSE06). These midgap states disappear

when the surface is allowed to reconstruct under full geometry relaxation.[70] We found that adsorption of a one molecule per surface unit monolayer of water also eliminates the midgap electronic states and increases the HOMO-LUMO energy gap to 3.54 eV (HSE06). In particular, projecting the density of states onto the surface atoms shows the predominant Ga character of the midgap electronic states (Fig. 3).

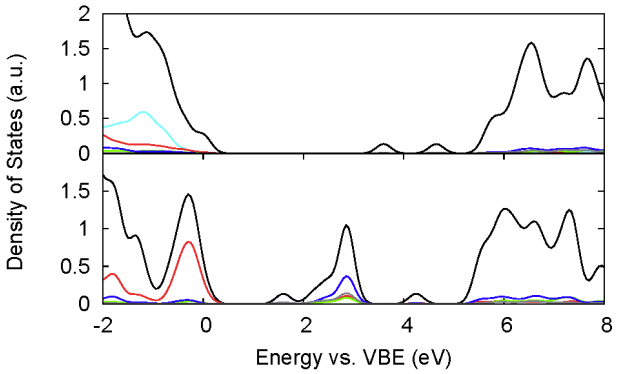

Figure 3: Density of states as obtained using HSE06 projected on surface atoms of GaN: (top) 1 ML-H_2O adsorbed on a 8 atomic layer thick slab GaN slab (monolayers on both sides) and (bottom) bare GaN 8 atomic layer thick slab. The color coding is the same as in Fig. 1. Note, unlike the geometry of the ML covered slab which has been fully relaxed, the bare slab has been simply cut out of the solid without any geometry relaxation.

All water molecules in the monolayer spontaneously dissociate with one OH^- bound to a surface Ga atom and one H^+ bound to a surface N atom. This is consistent with observations of previous work by Muckerman and coworkers.[21,22] Dissociation of the water monolayer seems to be capable of passivizing all midgap electronic states (Fig. 4). A similar result is observed for the clean $(10\bar{1}0)$ InN surface, with the HOMO-LUMO energy gap decreasing from 0.56 eV in a bulk structure to 0.27 eV for 8 atomic layers (HSE06). Mid-gap electronic states on surfaces $(10\bar{1}0)$ of $In_xGa_{1-x}N$ alloys of varying In content are also passivated by dissociative adsorption of a water monolayer.

We also note that replacing full solvation by a monolayer has a finite but small effect. Focus-

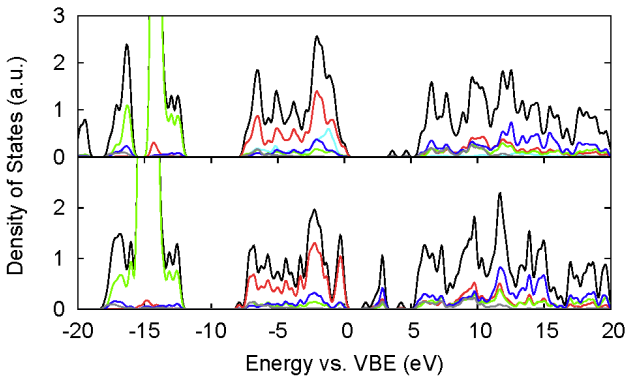

Figure 4: Density of states of 1 ML-H_2O adsorbed on the $(10\bar{1}0)$ surface of an 8 atomic layer thick slab of GaN (top) and corresponding clean surface (bottom) using the HSE06 hybrid functional. Zero energy is aligned to the VBE. The color coding is the same as in Fig. 1.

ing again on the performance of HSE06 we see that the HOMO and LUMO are approximately 0.4 V more positive compared to the band edges in full solvation (data in Table 1). Our shift is in good agreement with the estimate of 0.2V computed in Ref. 22(see also Table 1). A bulk solvation effect this small is somewhat unexpected for adsorption of a polar molecule such as H_2O and is presumably related to the surface induced dissociation.

Looking at the density of states for the water monolayer covered surface, the number of states is extremely low near the conduction band edge. Moreover, there is an absence of electronic states just above the LUMO. Projection of the density of states on the surface atoms does not flag the LUMO as a dangling bond state. However, the virtual orbitals are most likely extended free electron like states which are known to be more sensitive to system size effects (box quantization) than the more localized occupied states.[71] If this is the explanation, this should also show in the variation of the density of states of bulk GaN with supercell sizes. For bulk GaN with the same supercell size as the water monolayer adsorbed surface, the PBE LUMO state is even more isolated (Fig. 5). However, for larger supercell sizes, the number of states near the LUMO at the conduction band edge increases significantly (Fig. 5).

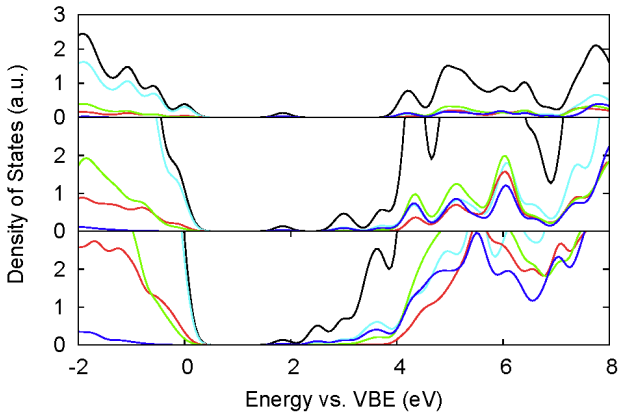

Figure 5: Density of states for bulk GaN using the PBE functional for different supercell sizes: (top) 9.5700Å × 10.3780Å × 11.0505Å (middle) 12.7600Å × 20.7560Å × 22.1010Å (bottom) 19.1400Å × 31.1340Å × 33.1515Å. The zero of energy is aligned to the VBE. The color legend is as follows: Green Ga4p, blue Ga4s, red Ga3d, turquoise N2p. The total density of states is indicated by the black curve.

Slab-thickness dependence

The thickness of a slab can be a critical parameter affecting the IP and EA. The question of system size dependence of the electronic structure has been examined in great detail for TiO_2.[72–75] Bare TiO_2 slabs show a pronounced odd-even oscillatory dependence on thickness. The effect persists to system sizes of well over 10 layers and is particularly sensitive to atomic relaxation.[73] However, adsorption of a single monolayer of H_2O, completing the six fold coordination of surface Ti ions, seems to be capable of suppressing the oscillations to the extent that they can be ignored for systems sizes accessible to DFTMD.[37]

System size dependence remains however a serious concern and we have therefore investigated the IP and EA of GaN and InN slabs of different thicknesses. The surfaces on both side are covered again with one monolayer of H_2O. The slabs are separated by a vacuum region . The vertical VBE and CBE were obtained by subtracting the electrostatic Hartree potential in the vacuum region from the HOMO and LUMO energies respectively (for more detail see model system section). The results are shown in Fig. 6. For comparison to the data in Table 1 and Fig. 2 ionization energies are given as potentials vs SHE by subtracting the experimental value for the absolute hydrogen electrode potential (4.44 V). First, we verified that band edge positions and band gaps follow similar trends whether the HSE06 hybrid functional or the PBE functional is used. The CBE in the HSE06 hybrid functional approximation was found at slightly more negative potentials than in the PBE functional. The HSE06 VBE was at more positive potentials compared to PBE. However, the differences between HSE06 and PBE for both materials are effectively independent of slab thickness.

Analyzing the GaN data first, we see that the CBE position remained largely constant over the range of slab thicknesses, varying between −0.97 V vs SHE and −0.56 V vs SHE, with even-odd oscillations not exceeding 0.3 V for the HSE06 hybrid functional (Fig. 6a). The VBE positions and band gap oscillated with even-odd layer numbers with amplitudes greater than 1 V for the HSE06 hybrid functional (Fig. 6a,b). However, comparing only even to and odd to odd layer systems, the VBE and CBE positions do not appear to change significantly with increasing thickness. For even numbers of atomic layers, the band gap appears to be converging rather quickly towards the bulk value of 2.98 eV. The finite size errors in the 8-layer model for GaN are therefore modest supporting the agreement with experiment in Table 1.

Next we turn to InN. The CBE and VBE positions oscillated with initial even-odd amplitudes of ≈ 1 V when computed using HSE06 (Fig. 6c). The potentials for the VBE and CBE became consistently more positive with increasing slab thickness. For PBE the VBE and CBE for 24 atomic layers are found 0.60 V and 0.94 V more positive than for 8 atomic layer system. Compared to GaN, InN band edge positions converge much slower for increasing slab thickness. The band gap shows variations between 0.69 eV and 1.14 eV, with variations not

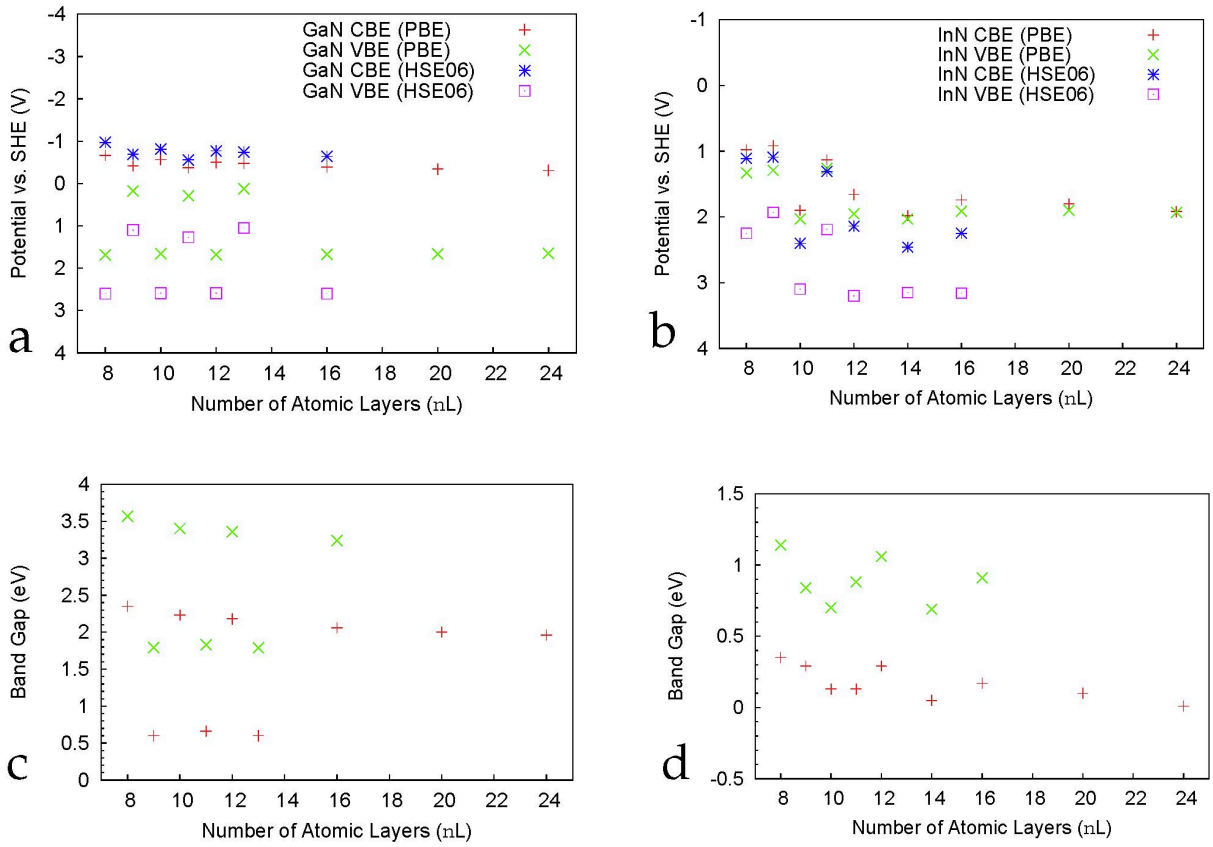

Figure 6: PBE and HSE06 hybrid results for the VBE and CBE positions as a function of the number of atomic layers (nL) of a slab covered with 1 ML H_2O. Ionization energies relative to vacuum have been converted to potentials vs SHE for easy comparison to estimates obtained for fully immersed slabs. Band edges for GaN are shown in a) GaN and for InN in b). The corresponding band gaps are shown in c) for GaN and d) for InN. Band gaps obtained using PBE are indicated by a red plus, band gaps obtained by HSE06 by a green cross.

exceeding 0.3 eV for the HSE06(Fig. 6d). In conclusion, the convergence tests for InN seem to indicate that restricting the model system to 8 layers leads to a cathodic bias of about $-1V$ which is a significant finite size error.

Composition dependence

Free energy calculation in full solution is too expensive to be carried out over a whole series of mixed $In_xGa_{1-x}N$ compounds. The effect of replacing full solvation by a monolayer can however be assessed for the terminal states $x = 0$ (GaN) and $x = 1$ (InN). From the data in Table 1 we saw that the effect is surprisingly small, only 0.3 V. Moreover the band gap is essentially preserved. Therefore, while water monolayers do not reproduce full water solvation, they provide a reasonably accurate first estimate of the shift of band edge positions in response to an increase in the In fraction in $In_xGa_{1-x}N$ alloys. The investigation of the effect of a variation of composition was therefore restricted to a comparison of HOMO and LUMO of H_2O monolayer slab geometries following the methodology used to check the system size dependence (see previous section).

The CBE and VBE of $In_{0.23}Ga_{0.77}N$, $In_{0.33}Ga_{0.67}N$, and $In_{0.61}Ga_{0.39}N$ have been calculated using both the PBE functional and the HSE06 hybrid functional (Fig. 7, Table 1). As the In content increases, the CBE position moves to more positive potentials. The change in potential is substantial from at -0.97 V vs

SHE according to HSE06 to 1.11 V vs. SHE for InN amounting to a more than 2 V anodic shift. PBE gives a very similar result. The VBE position moves to more negative potentials, but is much less sensitive to alloying.

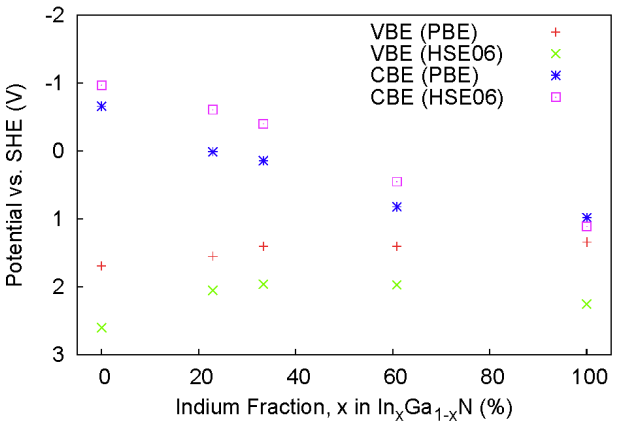

Figure 7: In fraction dependence of $In_xGa_{1-x}N$ band alignment. The In fraction x is represented as a percentage. Band edge positions are given in V vs SHE.

The density of states for $In_xGa_{1-x}N$ alloys for the selected set of x values are shown in Fig. 8. There is a continuous change in the conduction band character as the In content is increased. The main contribution to the density of states at the CBE in GaN comes from the Ga s orbitals. Substituting Ga for In narrows the band gap due to mixing of Ga s and In s orbitals (Fig. 8). The overall density of states at the CBE is similar in $In_xGa_{1-x}N$ alloys of all compositions. Also, the Ga p and In p contributions to the conduction band appear to vary continuously with increasing In content. In contrast, the character of the VBE is rather stable, with the main component being the N p orbitals regardless of composition. The decrease of the band gap due to mixing of the Ga and In electronic states is consistent with the band alignment calculations, which also indicate that the CBE moves to more positive potentials with respect to the VBE as In content increases.

Spin Density Localization

In this last section we finally address the question of excess electron and hole trapping. As

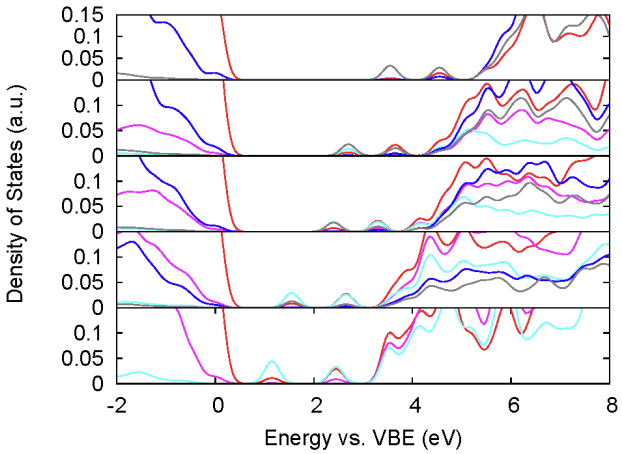

Figure 8: Density of states near the band edges for (top) GaN (second) $In_{0.23}Ga_{0.77}N$ (third) $In_{0.33}Ga_{0.67}N$ (fourth) $In_{0.61}Ga_{0.39}N$ (bottom) InN for the HSE06 hybrid functional. Zero energy is aligned to the VBE.The color legend is as follows: Magenta In5p, blue Ga4p, turquoise In5s, gray Ga4s, red N2p.

mentioned in the method section, localization of excess charge will lead to discrepancies between vertical band edges (Eqs. 10 and 11), in practice equal to HOMO and LUMO, and adiabatic band edges (Eq. 12 and 13). Covalent semiconductors show no spin polarization in the neutral groundstate. The spin density in the ionized state can therefore be interpreted as excess charge density. Spin densities for oxidized and reduced GaN are shown in Fig. 9. With spin density as a probe of excess charge density, we see that in singly ionized GaN^+, the hole is delocalized over the N atoms. While the hole is more localized for HSE06 (Fig. 9a) compared to PBE(Fig. 9b) the differences between functionals are again only minor. Similarly, the excess electron in GaN^- is delocalized over the Ga atoms with little difference between HSE06(Fig. 9c) and PBE(Fig. 9d). The observed spindensity distributions are consistent with he orbital resolution of the states at the bandedges (see Fig. 1). The delocalization of excess charge can also be seen as an explanation why the effect of full solvation on the structure of GaN and InN surfaces is little different from coverage by 1ML of water. There is little build up of net charge which could lead to long range solvation effects as observed in homogeneous so-

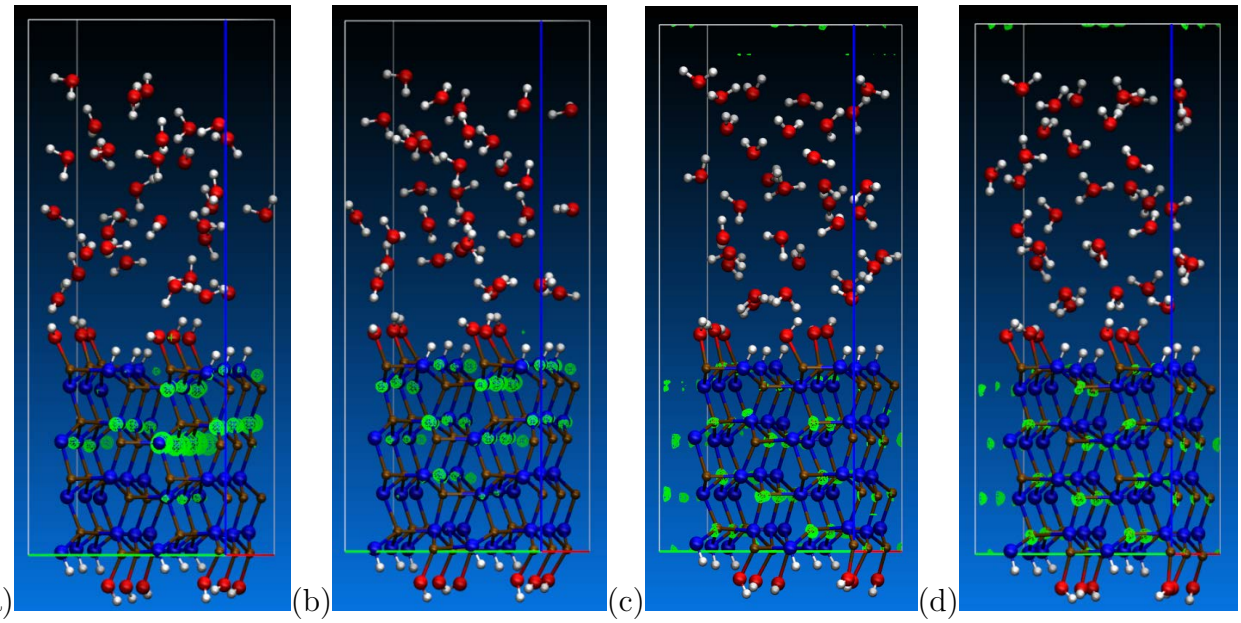

Figure 9: spin density plots for equilibrated a) GaN^+ (HSE06), b) GaN^+ (PBE), c) $GaN^- + H_3O^+$ (HSE06) and d) $GaN^- + H_3O^+$ (PBE). Red, white, blue, and gold spheres correspond to O, H, N, and Ga atoms. Spin isosurfaces are visualized in green. Spin isovalues of 1.0×10^{-4} (a, b) and 4.0×10^{-3} (c,d) were used.

lution.

Discussion

How do the calculated band edges compare to experiment? The experimental literature agrees that aqueous GaN interface potentials show a Nernstian dependence on pH.[11–13] This means that bandedge levels shift to higher (less negative) energies by 0.059 eV per pH unit (with very minor variations due to orientation). This property of aqueous GaN interfaces is the main reason why these systems have been considered for the construction of pH sensors using Ion Sensitive Field Effect Transistor (ISFET) technology.[14,15] The DFT calculations have been carried out for a charge neutral surface which would correspond to an experimental interface at the pH of zero charge (PZC, neglecting adsorption of all ions other than protons). We were unable to find an estimate of PZC in any of the experimental studies mentioned. However, Ref. 16 gives an indirect estimate based on a fit of a model of an ISFET to the measurements of Ref. 14. The PZC value obtained in Ref. 16 is a pH of 7, which is the pH we will use as the reference for the comparison of calculated bandedges to experiment.

Photocurrent measurements at pH 7 by Beach and co-workers place the VBE of n-type GaN at 2.55 V vs SHE and the CBE at −0.86 V vs. SHE[12] (these numbers can also be found in Table 1). Previous experiments by the same group gave 2.14 V for the VBE and −1.26 V for the CBE.[11] Interpolation of the values given by Huygens and coworkers[13] gives at pH = 7 a CBE at −1.0 V vs SHE and a VBE at 2.37 V vs SHE. These values are intermediate between those of Refs. 12 and 11 (see also Table 1. The band alignments obtained for both the water monolayer adsorbed system and for the fully solvated system using the HSE06 hybrid functional agree to within ≈ 10 percent of this range.

For InN the agreement is less satisfying. The band gap for the bulk solvated slab is 1.36 eV, which is significantly higher than the experimental value of 0.69 eV.[68] The band gap calculated for the monolayer adsorbed InN slab was 1.14 eV, which is also higher than 0.69 eV. As mentioned, slab thickness dependence, which for some reason is more pronounced for InN, is a possible cause for these deviations. Agree-

ment between calculated band gaps for InN and the experimental value improves with increasing number of atomic layers.

X-ray photoelectron spectroscopy experiments place the binding energy at the VBE of InN at 1.4 eV, with zero binding energy corresponding to the Fermi edge of Ag.[69] Assuming a value of 4.26 eV for the workfunction of Ag, this gives an experimental estimate for the VBE of InN at roughly 1.22 V vs SHE which is reproduced in Table 1. Comparing the calculated band edges and corresponding experimental values listed in Table 1 we find the VBE at 1.8 V for HSE06 vs 1.22 V experiment and the CBE at 0.44 for HSE06 vs 0.53 V from experiment. One might conclude therefore that discrepancies for InN are of the same order as for GaN (0.3 to 0.4 V). However, as mentioned earlier the InN IP and EA of the 8-layer system suffer from significant finite size errors. Adding the 1 V correction suggested by the convergence plots of Fig. 6 makes the agreement with experiment much worse for InN. The question that remains to be answered, however, is why the electronic structure of InN is more sensitive to finite size effects than for GaN.

Regarding the electronic structure we made a number of observations. First, water dissociation passivates mid-gap electronic states on $(10\bar{1}0)$ $In_xGa_{1-x}N$ surfaces, and second, equilibration of the surface opens up the band gap relative to the bulk. Passivation of $(10\bar{1}0)$ $In_xGa_{1-x}N$ dangling bonds is expected since dissociative water adsorption eliminates vacant surface coordination sites similarly to H^-, Cl^-, or F^- termination of Si or GaAs.[76,77] The increase in band gap due to water adsorption must probably again be attributed to slab-thickness dependence of the electronic structure. It is hard to see how surface effects can have any other effect on the band gap than decreasing it.

After these more technical observations, we come to the main physical result of the calculation. The In content dependence of the CBE position in water monolayer adsorbed $In_xGa_{1-x}N$ is observed to be linear. Fitting the data, we find CBE $= -1.03 + 2.19x$ eV vs SHE, where x is the In fraction, with correlation coefficient $R^2 = 0.98$. Using these fitted values for the CBE of $In_xGa_{1-x}N$, the band edges will straddle the hydrogen and oxygen evolution potentials, allowing water splitting, for up to 47 percent In fraction. The valence band offset is small, a few tenths of an eV, as expected since GaN and InN share a common anion. The In content dependence of the band gap in water monolayer adsorbed $In_xGa_{1-x}N$ systems is also observed to be linear. Fitting the data, $E_g = 3.30 - 2.41x$ eV, where x is the In fraction, with correlation coefficient $R^2 = 0.99$. Recalling that water splitting photoelectrodes need a band gap of approximately 2 eV, we predict that $In_xGa_{1-x}N$ with In fraction up to 54 percent will satisfy this requirement. Based on our calculations, $In_xGa_{1-x}N$ with In fraction less than ≈ 50 percent satisfies both the band gap and band position requirements for water splitting. One main assumption for this result is that the In substitution in the $In_xGa_{1-x}N$ is approximately uniform.

Conclusion

Using density functional theory based MD, we were able to account for the alignment of $(10\bar{1}0)$ $In_xGa_{1-x}N/H_2O$ interfaces. Band edge positions of unalloyed aqueous GaN and InN compounds were computed directly with respect to the standard hydrogen electrode using the work function of the proton as reference. The model system in this approach is a periodic heterogeneous solid/liquid system without an interface to vacuum. The proton work function is computed from the reversible work for inserting a proton in the aqueous part of the model system. This relatively expensive calculation was used to validate the more computationally efficient method of estimating the band edge positions from HOMO-LUMO energies of a vacuum system consisting of a slab covered with one monolayer of water on both sides.

For GaN, VBE and CBE values agree well with flat-band potential and band gap measurements from experiment. Using the simplified minimally hydrated slab, we find that the CBE moves linearly from -0.97 V vs. SHE for GaN

to 1.11 V vs SHE for InN with increasing In content. While this agrees well with x-ray photoelectron spectroscopic experiments, we remind the reader that the 1.11 V CBE at the InN end must be considered a lower bound due to finite size errors.

The accuracy of the DFT approximation, of course, remains a major concern. This is evident comparing the results of the two DFT protocols listed in Table 1. The PBE ionization energies for GaN are underestimated by as much as 1 eV. Application of HSE06 brings significant improvement, which can be interpreted as confirmation that accounting for Hartree Fock exchange is necessary. However, the GW calculation of Ref. 22, based on screened full exact exchange, leads to overestimation of the GaN IP in the order of 0.5 eV relative to experiment. We leave the analysis of this observation to the experts in many-body theory.

Unfortunately, in addition to finite system size effects, a further complication for a proper assessment of the electronic structure calculation scheme is that the alignment of energy levels, either with respect to the SHE or vacuum, is still far from an established procedure. Our MDHE and the method applied in Ref. 22 are sufficiently different that discrepancies of 0.5 eV cannot be excluded. The proton insertion method at the core of the MDHE may seem an expensive and less direct method compared to the vacuum level alignment used in Ref. 22 (see also Ref. 34). However, as already pointed out in the general section on the MDHE method, the major advantage of proton insertion is that it can be validated using pKa calculation in homogeneous solution for which the DFT can be considered relatively safe.[38,45,47]

The hydrogen insertion method can be applied to band alignment of other multicomponent water splitting catalysts including GaN:ZnO alloys and ternary oxides. The calculations on $Ga_xIn_{1-x}N$ presented here seem to suggest that the HSE06 hybrid functional is sufficient to provide estimates for band positions. This positive evaluation must however almost certainly be restricted to d^{10} compounds, such as GaN, and d^0 compounds such as TiO_2. Mid-period transition metal oxides with partial d shell occupation (the notorious example is Fe_2O_3) introduce another category of difficulty related to strong correlations. However d^0 and d^{10} materials are of major interest for photovoltaics and photocatalysis, and here density functional theory based MD seems to provide a systematic approach to examine the surface chemistry of band alignment while also providing guidance for experiments on multicomponent materials.

Acknowledgement

ACM is grateful to the Winston Churchill foundation of the United States for a scholarship. The computations were carried out on the Archer facility of the National Supercomputer Service of the United Kingdom using the computer time allocation of the UK Car-Parrinello consortium (UKCP).

Supporting Information Available

A more detailed explanation of the MDHE scheme for alignment of the VBE and CBE is given using he HSE06 results in Table 1 as example.

References

(1) Gerischer, H. On the Stability of Semiconductor Electrodes against Photodecomposition. *J. Electroanal. Chem.* **1982**, *77*, 133–143.

(2) Maeda, K.; Takata, T.; Hara, M.; Saito, N.; Inoue, Y.; Kobayashi, H.; Domen, K. GaN:ZnO Solid Solution as a Photocatalyst for Visible-Light-Driven Overall Water Splitting. *J. Am. Chem. Soc.* **2005**, *127*, 8286–8287.

(3) Maeda, K.; Domen, K. New Non-Oxide Photocatalysts Designed for Overall Water Splitting under Visible Light. *J. Phys. Chem. C* **2007**, *111*, 7851–7861.

(4) Moriya, Y.; Takata, T.; Domen, K. Recent Progress in the Development of (Oxy)Nitride Photocatalysts for Water

Splitting under Visible-Light Irradiation. *Coor. Chem. Rev.* **2013**, *257*, 1957–1969.

(5) Fujii, K.; Usakabe, K.; Ohkawa, K. Photoelectrochemical Properties of InGaN for H_2 Generation from Aqueous Water. *Jpn. J. Appl. Phys.* **2005**, *44*, 7433–7435.

(6) Kida, T.; Minami, Y.; Guan, G.; Nagano, M.; Akiyama, M.; Yoshida, A. Photocatalytic Activity of Gallium Nitride for Producing Hydrogen from Water under Light Irradiation. *J. Mater. Sci.* **2006**, *12*, 3527–3534.

(7) Jung, H. S.; Hong, Y. J.; Li, Y.; Cho, J.; Kim, Y.-J.; Yi, G.-C. Photocatalysis Using GaN Nanowires. *ACS nano* **2008**, *2*, 637–642.

(8) Wang, D.; Pierre, A.; Kibria, M. G.; Cui, K.; Han, X.; Bevan, K. H.; Guo, H.; Paradis, S.; Hakima, A.-R.; Mi, Z. Wafer-Level Photocatalytic Water Splitting on GaN Nanowire Arrays Grown by Molecular Beam Epitaxy. *Nano Lett.* **2011**, *11*, 2353–2357.

(9) Hwang, Y. J.; Wu, C. H.; Hahn, C.; Jeong, H. E.; Yang, P. Si/InGaN Core/Shell Hierarchical Nanowire Arrays and their Photoelectrochemical Properties. *Nano Lett.* **2012**, *12*, 1678–1682.

(10) Schäfer, S.; Koch, A. H. R.; Cavallini, A.; Stutzmann, M.; Sharp, I. D. Charge Transfer across the n-Type GaN-Electrolyte Interface. *J. Phys. Chem. C* **2012**, *116*, 22281–22286.

(11) Kocha, S. S.; Peterson, M. W.; Arent, D. J.; Redwing, J. M.; Tischler, M. A.; Turner, J. A. Electrochemical Investigation of the Gallium Nitride-Aqueous Electrolyte Interface. *J. Electrochem. Soc.* **1995**, *150*, L238–L240.

(12) Beach, J. D.; Collins, R. T.; Turner, J. A. Band-Edge Potentials of n-Type and p-Type GaN. *J. Electrochem. Soc.* **2003**, *150*, A899–A904.

(13) Huygens, I. M.; Strubbe, K.; Gomes, W. P. Electrochemistry and Photoetching of n-GaN. *J. Electrochem. Soc.* **2000**, *147*, 1797–1802.

(14) Steinhoff, G.; Hermann, M.; Schaff, W. J.; Eastman, L. F.; Stutzmann, M.; Eickhoff, M. pH Response of GaN Surfaces and its Application for pH-Sensitive Field-Effect Transistors. *Appl. Phys. Lett.* **2003**, *83*, 177–179.

(15) Wallys, J.; Teubert, J.; Furtmayr, F.; Hofmann, D. M.; Eickhoff, M. Bias-Enhanced Optical pH Response of Group III—Nitride Nanowires. *Nano Lett.* **2012**, *12*, 6180—6186.

(16) Bayer, M.; Uhl, C.; Vogl, P. Theoretical Study of Electrolyte Gate AlGaN/GaN Field Effect Transistors. *J. Appl. Phys.* **2005**, *97*, 033703.

(17) Shen, X.; Allen, P. B.; Hybertsen, M. S.; Muckerman, J. T. Water Adsorption on the GaN $(10\bar{1}0)$ Nonpolar Surface. *J. Phys. Chem. C* **2009**, *113*, 3365–3368.

(18) Shen, X.; Small, Y. A.; Wang, J.; Allen, P. B.; Fernandez-Serra, M. V.; Hybertsen, M. S.; Muckerman, J. T. Photocatalytic Water Oxidation at the GaN $(10\bar{1}0)$-Water Interface. *J. Phys. Chem. C* **2010**, *114*, 13695–13704.

(19) Wang, J.; Pedroza, L. S.; Poissier, A.; Fernandez-Serra, M. V. Water Dissociation at the GaN $(10\bar{1}0)$ Surface: Structure, Dynamics and Surface Acidity. *J. Phys. Chem. C* **2012**, *116*, 14382—14389.

(20) Akimov, A. V.; Muckerman, J. T.; Prezhdo, O. V. Nonadiabatic Dynamics of Positive Charge during Photocatalytic Water Splitting on GaN $(10\bar{1}0)$ Surface: Charge Localization Governs Splitting Efficiency. *J. Am. Chem. Soc.* **2013**, *135*, 8682—8691.

(21) Kharche, N.; Hybertsen, M. S.; Muckerman, J. T. Computational Investigation of Structural and Electronic Properties of Aqueous Interfaces of GaN, ZnO, and a GaN/ZnO Alloy. *Phys. Chem. Chem. Phys* **2014**, *16*, 12057–12066.

(22) Kharche, N.; Muckerman, J. T.; Hybertsen, M. S. First-Principles Approach to Calculating Energy Level Alignment at Aqueous Semiconductor Interfaces. *Phys. Rev. Lett.* **2014**, *113*, 176802.

(23) Ertem, M. Z.; Kharche, N.; Batista, V. S.; Hybertsen, M. S.; Tully, J. C.; Muckerman, J. T. Photoinduced Water Oxidation at the Aqueous GaN $(10\bar{1}0)$ Interface: Deprotonation Kinetics of the First Proton-Coupled Electron-Transfer Step. *ACS Catal.* **2015**, *5*, 2317–2323.

(24) Ping, Y.; Rocca, D.; Galli, G. Electronic Excitations in Light Absorbers for Photoelectrochemical Energy Conversion: First Principles Calculations Based on Many Body Perturbation Theory. *Chem. Soc. Rev.* **2013**, *42*, 2437–2469.

(25) Ping, Y.; Galli, G. Optimizing the Band Edges of Tungsten Trioxide for Water Oxidation: A First-Principles Study. *J. Phys. Chem. C* **2014**, *118*, 6019–6028.

(26) Liao, P.; Carter, E. A. New Concepts and Modeling Strategies to Design and Evaluate Photo-Electro-Catalysts Based on Transition Metal Oxides. *Chem. Soc. Rev.* **2013**, *42*, 2401–2422.

(27) De Angelis, F.; Di Valentin, C.; Fantacci, S.; Vittadini, A.; Selloni, A. Theoretical Studies on Anatase and Less Common TiO_2 Phases: Bulk, Surfaces, and Nanomaterials. *Chem. Rev.* **2014**, *114*, 9708–9753.

(28) Migani, A.; Mowbray, D. J.; Zhao, J.; Petek, H. Quasiparticle Interfacial Level Alignment of Highly Hybridized Frontier Levels: H_2O on TiO_2(110). *J. Chem. Theor. Comp.* **2015**, *11*, 239–251.

(29) VandeWalle, C. G.; Martin, R. Theoretical Study of Band Offsets at Semiconductor Interfaces. *Phys. Rev. B* **1987**, *35*, 8154–8165.

(30) Baldereschi, A.; Baroni, S.; Resta, R. Bandoffsets in Lattice-Matched Heterojunctions: A Model and First-Principles Calculations for GaAs/AlAs. *Phys. Rev. Lett.* **1988**, *1961*, 734–737.

(31) Franciosi, A.; VandeWalle, C. G. Heterojunction Band Offset Engineering. *Surf. Sci. Rep* **1996**, *25*, 1–140.

(32) Junquera, J.; Cohen, M. H.; Rabe, K. M. Nanoscale Smoothing and the Analysis of Interfacial Charge and Dipolar Densities. *J. Phys.: Condens. Matter* **2007**, *19*, 213203.

(33) Pham, T. A.; Lee, D.; Schwegler, E.; Galli, G. Interfacial Effects on the Band Edges of Functionalized Si Surfaces in Liquid Water. *J. Am. Chem. Soc.* **2014**, *136*, 17071—17077.

(34) Pham, T. A.; Zhang, C.; Eric Schwegler, E.; Galli, G. Probing the Electronic Structure of Water with Many-body Perturbation Theory. *Phys. Rev. B* **2014**, *89*, 060202(R).

(35) Wu, Y.; Chan, M. K. Y.; Ceder, G. Prediction of Semiconductor Band Edge Positions in Aqueous Environments from First Principles. *Phys. Rev. B* **2011**, *83*, 235301.

(36) Stevanovic, V.; Lany, S.; Ginley, D. S.; Tumas, W.; Zunger, A. Assessing Capability of Semiconductors to Split Water Using Ionization Potentials and Electron Affinities Only. *Phys. Chem. Chem. Phys* **2014**, *16*, 3706–3714.

(37) Cheng, J.; Sprik, M. Aligning Electronic Energy Levels at the TiO_2/H_2O Interface. *Phys. Rev. B* **2010**, *82*, 081406(R).

(38) Cheng, J.; Sprik, M. Alignment of Electronic Energy Levels at Electrochemical Interfaces. *Phys. Chem. Chem. Phys* **2012**, *14*, 11245–11267.

(39) Segev, D.; Janotti, A.; Van de Walle, C. G. Self-Consistent Band-Gap Corrections in Density Functional Theory Using Modified Pseudopotentials. *Phys. Rev. B* **2007**, *75*, 035201.

(40) Moses, P. G.; Van de Walle, C. G. Band Bowing and Band Alignment in InGaN Alloys. *Appl. Phys. Lett.* **2010**, *96*, 021908.

(41) Moses, P. G.; Miao, M.; Yan, Q.; Van de Walle, C. G. Hybrid Functional Investigations of Band Gaps and Band Alignments for AlN, GaN, InN, and InGaN. *J. Chem. Phys.* **2011**, *134*, 084703.

(42) Trasatti, S. The Absolute Electrode Potential: An Explanatory Note. *Pure & Appl. Chem.* **1986**, *58*, 955–966.

(43) Liu, X.; Cheng, J.; Sprik, M. Aqueous Transition-Metal Cations as Impurities in a Wide Gap Oxide: The Cu^{2+}/Cu^{+} and Ag^{2+}/Ag^{+} Redox Couples Revisited. *J. Phys. Chem. B* **2015**, *119*, 1152–1163.

(44) Cheng, J.; Sulpizi, M.; Sprik, M. Redox Potentials and pKa for Benzoquinone from Density Functional Theory Based Molecular Dynamics. *J. Chem. Phys.* **2009**, *131*, 154504.

(45) Costanzo, F.; Della Valle, R. G.; Sulpizi, M.; Sprik, M. The Oxidation of Tyrosine and Tryptophan Studied by a Molecular Dynamics Normal Hydrogen Electrode. *J. Chem. Phys.* **2011**, *134*, 244508.

(46) Adriaanse, C.; Cheng, J.; Chau, V.; Sulpizi, M.; VandeVondele, J.; Sprik, M. Aqueous Redox Chemistry and the Electronic Band Structure of Liquid Water. *J. Phys. Chem. Lett.* **2012**, *3*, 3411–3415.

(47) Cheng, J.; Liu, X.; VandeVondele, J.; Sulpizi, M.; Sprik, M. Redox Potentials and Acidity Constants from Density Functional Theory Based Molecular Dynamics. *Acc. Chem. Res.* **2014**, *47*, 3522–3529.

(48) Opalka, D.; Pham, T. A.; Sprik, M.; Galli, G. The Ionization Potential of Aqueous Hydroxide Computed Using Many-Body Perturbation Theory. *J. Chem. Phys.* **2014**, *141*, 034501.

(49) Opalka, D.; Pham, T. A.; Sprik, M.; Galli, G. Electronic Energy Levels and Band Alignment for Aqueous Phenol and Phenolate from First Principles. *J. Phys. Chem. B* **2015**, *119*, 9651–9660.

(50) Cheng, J.; Sprik, M. Acidity of the Aqueous Rutile TiO_2(110) Surface from Density Functional Theory Based Molecular Dynamics. *J. Chem. Theor. Comp.* **2010**, *6*, 880–889.

(51) Cheng, J.; Liu, X.; VandeVondele, J.; Sulpizi, M.; Sprik, M. Aligning Electronic and Protonic Energy Levels of Proton-Coupled Electron Transfer in Water Oxidation on Aqueous TiO_2. *Angew. Chem., Int. Ed. Engl.* **2014**, *53*, 12046–12050.

(52) Sulpizi, M.; Gaigeot, M.-P.; Sprik, M. The Silica-Water Interface: How the Silanols Determine the Surface Acidity and Modulate the Water Properties. *J. Chem. Theor. Comp.* **2012**, *8*, 137–147.

(53) Liu, X.; Cheng, J.; Sprik, M.; Lu, X.; Wang, R. Understanding Surface Acidity of Gibbsite with First Principles Molecular Dynamics Simulations. *Geochim. Cosmochim. Acta* **2013**, *120*, 487–495.

(54) Liu, X.; Lu, X.; Sprik, M.; Cheng, J.; Meijer, E. J.; Wang, R. Acidity of Edge Surface Sites of Montmorillonite and Kaolinite. *Geochim. Cosmochim. Acta* **2013**, *117*, 180–190.

(55) King, G.; Warshel, A. Investigation of the Free Energy Functions for Electron Transfer Reactions. *J. Chem. Phys.* **1990**, *93*, 8682–8692.

(56) Sulpizi, M.; Sprik, M. Acidity Constants from Vertical Energy Gaps: Density Functional Theory Based Molecular Dynamics Implementation. *Phys. Chem. Chem. Phys* **2008**, *10*, 5238–5249.

(57) Cheng, J.; VandeVondele, J.; Sprik, M. Identifying Trapped Electronic Holes at the Aqueous TiO_2 Interface. *J. Phys. Chem. C* **2014**, *118*, 5437–5444.

(58) Bard, A. J.; Bocarsly, A. B.; Fan, F.-R. F.; Walton, E. G.; Wrighton, M. S. The Concept of Fermi Level Pinning at Semiconductor/Liquid Junctions. Consequences for Energy Conversion Efficiency and Selection of Useful Solution Redox Couples in Solar Devices. *J. Am. Chem. Soc.* **1980**, *102*, 3671–3677.

(59) The CP2K Developers Group, `http://www.cp2k.org`, 2014.

(60) Hutter, J.; Iannuzzi, M.; Schiffmann, F.; VandeVondele, J. CP2K : Atomistic Simulations of Condensed Matter Systems. *WIREs Comput. Mol. Sci.* **2014**, *4*, 15–25.

(61) Goedecker, S.; Teter, M.; Hutter, J. Separable Dual-Space Gaussian Pseudopotentials. *Phys. Rev. B* **1996**, *54*, 1703.

(62) Hartwigsen, C.; Goedecker, S.; Hutter, J. Relativistic Separable Dual-Space Gaussian Pseudopotenials from H to Rn. *Phys. Rev. B* **1998**, *58*, 3641.

(63) Perdew, J. P.; Burke, K.; Ernzerhof, M. Generalized Gradient Approximation Made Simple. *Phys. Rev. Lett.* **1996**, *77*, 3865–3868.

(64) Krukau, A. V.; Vydrov, O. A.; Izmaylov, A. F.; Scuseria, G. E. Influence of the Exchange Screening Parameter on the Performance of Screened Hybrid Functionals. *J. Chem. Phys.* **2006**, *125*, 224106.

(65) Guidon, M.; Hutter, J.; VandeVondele, J. Auxiliary Density Matrix Methods for Hartree-Fock Exchange Correlations. *J. Chem. Theor. Comp.* **2010**, *6*, 2348–2364.

(66) Yeh, C.-Y.; Lu, Z. W.; Froyen, S.; Zunger, A. Zinc-Blende Wurtzite Polytypism in Semiconductors. *Phys. Rev. B* **1992**, *46*, 10086–10097.

(67) Chiou, W.; Mookerjee, S.; Rao, K. V. R.; Jan, J. C.; Tsai, H. M.; Asokan, K.; Pong, W. F.; Chien, F. Z.; Tsai, M.-H.; Chang, Y. K. et al. Angle-Dependent X-Ray Absorption Spectroscopy Study of Zn-Doped GaN. *Appl. Phys. Lett.* **2002**, *81*, 3389–3391.

(68) Wu, J.; Walukiewicz, W.; Shan, W.; Yu, K. M.; Ager, J. W.; Li, S. X.; Haller, E. E.; Lu, H.; Schaff, W. J. Temperature Dependence of the Fundamental Band Gap of InN. *J. Appl. Phys.* **2003**, *94*, 4457–4460.

(69) Piper, L. F. J.; Veal, T. D.; Jefferson, P. H.; McConville, C. F.; Fuchs, F.; Furthmüller, J.; Bechstedt, F.; Lu, H.; Schaff, W. J. Valence-Band Structure of InN from X-Ray Photoemission Spectroscopy. *Phys. Rev. B* **2005**, *72*, 245319.

(70) Northrup, J. E.; Neugebauer, J. Theory of GaN ($\mathbf{10\bar{1}0}$) and ($\mathbf{11\bar{2}0}$) surfaces. *Phys. Rev. B* **1996**, *53*, R10477.

(71) Prendergast, D.; Grossman, J. C.; Galli, G. The Electronic Structure of Liquid Water within Density-Functional Theory. *J. Chem. Phys.* **2005**, *123*, 014501.

(72) Murugan, P.; Kumar, V.; Kawazoe, Y. Thickness Dependence of the Atomic and Electronic Structures of TiO_2 Rutile (110) Slabs and the Effects on the Electronic and Magnetic Properties of Supported Clusters of Pd and Rh. *Phys. Rev. B* **2006**, *73*, 075401.

(73) Kowalski, P. M.; Meyer, B.; Marx, D. Composition, Structure, and Stability of

the Rutile TiO_2(110) Surface: Oxygen Depletion, Hydroxylation, Hydrogen Migration, and Water Adsorption. *Phys. Rev. B* **2009**, *79*, 115410.

(74) Liu, L.-M.; Zhang, C.; Thornton, G.; Michaelides, A. Structure and Dynamics of Liquid Water on Rutile TiO_2(110). *Phys. Rev. B* **2010**, *82*, 161415(R).

(75) He, T.; Li, J. L.; Yang, G. W. Physical Origin of General Oscillation of Structure, Surface Energy, and Electronic Property in Rutile TiO_2 Nanoslab. *ACS Appl. Mater. Interfaces* **2012**, *4*, 2192–2198.

(76) VandeWalle, C. G. Energies of Various Configurations of Hydrogen in Silicon. *Phys. Rev. B* **1994**, *49*, 4579–4585.

(77) Wang, W.; Lee, G.; Huang, M.; Wallace, R. M.; Cho, K. First-Principles Study of GaAs($\mathbf{001}$) $-\beta(\mathbf{2\times4})$ Surface Oxidation and Passivation with H, Cl, S, F, and GaO. *J. Appl. Phys.* **2010**, *107*, 103720.

Supporting information for: Density Functional Theory Calculation of the Band Alignment of $(10\bar{1}0)$ $In_xGa_{1-x}N$/Water Interfaces

Andrew C. Meng,[†,‡] Jun Cheng,[¶] and Michiel Sprik[*,†]

Department of Chemistry, University of Cambridge, Cambridge CB2 1EW, United Kingdom, Department of Materials Science and Engineering, Stanford University, CA 94305-4034, United States, and Department of Chemistry, University of Aberdeen, Aberdeen AB24 3UE, United Kingdom

E-mail: ms284@cam.ac.uk

Phone: +44-1223-336314. Fax: +44-1223-336362

[*]To whom correspondence should be addressed
[†]University of Cambridge
[‡]Stanford University
[¶]University of Aberdeen

The DFTMD calculation of the valence band edge (VBE) and conduction band edge (CBE) of the fully solvated model systems listed in Table 1 of the main text follows the procedure outlined in detail in previous technical papers. The method was developed for the DFTMD computation of the equilibrium constants of homogeneous acid-base and redox reactions[S1–S3] and was subsequently extended to heterogeneous systems.[S4] The relevant equations are given in the method section. The practical implementation of these equations will be illustrated here for the example of the HSE06 bandedges for GaN and InN. For a detailed explanation we refer to the original publications. The necessary data are summarized in Table S1. This includes the vertical gaps not given in the main text.

Table S1: MD averaged vertical energy gaps $\langle \Delta E \rangle_\eta$ and corresponding thermodynamic integrals $\int_0^1 d\eta \langle \Delta E \rangle_\eta$ used to compute the HSE06 results for the fully solvated GaN and InN systems given in Table 1 of the main text. The thermodynamic integrals have been obtained from the vertical energies using Eq. 3 (see text). Units are eV. The pbc qualifier added in brackets indicates that the energies have been computed from total energy differences of model systems under full periodic boundary conditions. X stands for the solvated neutral slab. $q = 0$ in the calculation of the VBE and CBE as carried out here.

		$\langle \Delta E(\text{pbc}) \rangle_\eta$			$\int_0^1 d\eta \langle \Delta E(\text{pbc}) \rangle_\eta$
	η	0.0	0.5	1.0	
GaN	$X^q \rightarrow X^{q+1} + e^-$	0.42	0.33	−0.01	$\text{AIP}_q(\text{pbc}) = 0.27$
	$H_3O^+ \rightarrow H_2O + H^+$	20.97	18.76	13.90	$W_{H^+}(\text{pbc}) = 18.10$
	$X_{q-1} + H_3O^+ \rightarrow X_q + H_2O + e^- + H^+$	18.45	14.96	10.78	$\text{AEA}_q + W_{H^+} = 14.79$
InN	$X^q \rightarrow X^{q+1} + e^-$	0.10	−0.31	−1.00	$\text{AIP}_q(\text{pbc}) = -0.38$
	$H_3O^+ \rightarrow H_2O + H^+$	20.60	18.96	14.84	$W_{H^+}(\text{pbc}) = 18.34$
	$X_{q-1} + H_3O^+ \rightarrow X_q + H_2O + e^- + H^+$	19.37	16.74	13.53	$\text{AEA}_q + W_{H^+} = 16.60$

Following the generalized notation of the technical summary of the MDHE method, the neutral solid is indicated by X^q with $q = 0$. The ionization reaction $X^q \rightarrow X^{q+1} + e^-$ and hydronium deprotonation $H_3O^+ \rightarrow H_2O + H^+$ are half reactions. The corresponding vertical energies are directly obtained from total energy differences under periodic boundary conditions (pbc). For the ionization reaction the energy gap ΔE is the vertical ionization

potential IP and is computed as

$$\Delta E_q = E_{q+1} - E_q \tag{1}$$

where E_{q+1} and E_q are the total energy of the ionized and neutral system respectively (recall $q = 0$). ΔE_q is specific to the composition of the model system.

The computation of the vertical energy gap for deprotonation of an hydronium, $H_3O^+ \rightarrow H_2O + H^+$ is again based on total energy differences for fixed ionic configurations, one configuration having one proton more than the other. The proton is however not completely removed. Instead its charge is set to zero turning it into a "ghost" proton H^* invisible to all charge in the system but still attached to the reactant hydronium by a harmonic potential. We can therefore write

$$\Delta E_{H_3O^+} = E_{H_3O^+} - E_{H_2OH^*} \tag{2}$$

where $E_{H_3O^+}$ is the total energy of the system containing a certain number of water molecules plus the solid slab and one single hydronium ion H_3O^+ placed in the middle of the water zone away from the surface. $E_{H_2OH^*}$ is the total energy of the system with one of the three hydronium protons exchanged for a charge neutral ghost proton. Technical details of this procedure can be found in Refs. S1 and S2. The method has been validated by comparing the computed pKa of a number of small acids to experiment.[S2,S3] The experimental values could be reproduced within 2 pK units corresponding to an uncertainty of 0.10 - 0.15 eV.

The instantaneous vertical gap ΔE is averaged over MD trajectories generated by the mapping Hamiltonian Eq. 2 for a set of values of the coupling parameter η. The resulting time average is indicated by $\langle \Delta E \rangle_\eta$ in Table S1. Because of the computational costs of HSE06 calculations the number of η values is limited to three ($\eta = 0.0, 0.5, 1$). This leads to a three point numerical estimate of the thermodynamic integral $\int_0^1 d\eta \langle \Delta E \rangle_\eta$. The three point approximation used here is the trapezium rule

$$\int_0^1 d\eta \langle \Delta E \rangle_\eta = \frac{h}{2} \left(\langle \Delta E \rangle_{\eta=0} + \langle \Delta E \rangle_{\eta=0.5} \right) + \frac{h}{2} \left(\langle \Delta E \rangle_{\eta=0.5} + \langle \Delta E \rangle_{\eta=1.0} \right) \tag{3}$$

with interval width $h = 0.5$. Note that the three point approximation used in our previous publications is the Simpson rule

$$\int_0^1 d\eta \langle \Delta E \rangle_\eta = \frac{1}{6} \left(\langle \Delta E \rangle_{\eta=0} + \langle \Delta E \rangle_{\eta=1} \right) + \frac{2}{3} \langle \Delta E \rangle_{\eta=0.5} \tag{4}$$

which gives an end point ($\eta = 0.0, 1.0$) a slightly smaller weight (1/6 instead of the 1/4 of Eq. 3). The differences in the estimate of the thermodynamic integrals are however small.

The thermodynamic integral $W_{\mathrm{H^+}}(\mathrm{pbc}) = 18.10$ eV in Table S1 is the proton workfunction of Eq. 7 for the GaN model system. Combining with the constants $\mu^{g,\circ}_{\mathrm{H^+}} = 15.81$ eV and $\Delta E_{\mathrm{zp}} = 0.35$ and substituting in Eq. 6 we obtain the MDHE potential $U^{\circ}_{\mathrm{H^+/H_2}}(\mathrm{pbc}) = -1.94$ V. We repeat the warning that this is not an universal parameter, but specific to the chosen GaN model system. $\mathrm{AIP}_q(\mathrm{pbc}) = 0.27$ eV of Table S1 is the adiabatic ionization potential of Eq. 3 of the main text. Substituting in Eq. 12 we recover the adiabatic GaN VBE at 1.21 V vs SHE listed for HSE in Table 1 of the main text.

To obtain the corresponding CBE the electron and proton have been inserted simultaneously applying what we called the full reaction scheme. Separate calculation of the adiabatic electron affinity $\mathrm{AEA}_q(\mathrm{pbc})$ and $W_{\mathrm{H^+}}(\mathrm{pbc})$ is avoided. We directly obtain the sum $\mathrm{AEA}_q + W_{\mathrm{H^+}}$ which is not affected by the uncertainty in the electrostatic reference potential (hence we have omitted the (pbc) argument) but still, of course, sensitive to finite system system size errors. All what is needed is to subtract the constant offset $\mu^{g,\circ}_{\mathrm{H^+}} + \Delta E_{\mathrm{zp}} = 16.16$ eV from the $\mathrm{AEA}_q + W_{\mathrm{H^+}} = 14.79$ eV estimate of Table S1 and we obtain the -1.37 V SHE alignment of the GaN CBE in Table 1 of the main text.

The full reaction scheme has certain advantages over the half reaction scheme because systems with net total charge are avoided. The full reaction scheme for calculation of the VBE is however more involved. Removing an electron and proton from the neutral system leaves it with a hole in the solid and an $\mathrm{OH^-}$ ion. To transform to the SHE potential a separate calculation of the dissociation constant (pKw) of water is needed. This calculation

has been carried out for pure water.[S3] While this result should in principle be transferable to "bulk" water in heterogeneous systems, finite system size errors are in practice a complication, which is why we have used the half reaction scheme to determine the VBE.

References

(S1) Cheng, J.; Sulpizi, M.; Sprik, M. Redox Potentials and pKa for Benzoquinone from Density Functional Theory Based Molecular Dynamics. *J. Chem. Phys.* **2009**, *131*, 154504.

(S2) Costanzo, F.; Della Valle, R. G.; Sulpizi, M.; Sprik, M. The Oxidation of Tyrosine and Tryptophan Studied by a Molecular Dynamics Normal Hydrogen Electrode. *J. Chem. Phys.* **2011**, *134*, 244508.

(S3) Cheng, J.; Liu, X.; VandeVondele, J.; Sulpizi, M.; Sprik, M. Redox Potentials and Acidity Constants from Density Functional Theory Based Molecular Dynamics. *Acc. Chem. Res.* **2014**, *47*, 3522–3529.

(S4) Cheng, J.; Sprik, M. Alignment of Electronic Energy Levels at Electrochemical Interfaces. *Phys. Chem. Chem. Phys* **2012**, *14*, 11245–11267.